Biosensors and Bioelectronics ■ (■■■■) ■■■–■■■

Contents lists available at ScienceDirect

Biosensors and Bioelectronics

journal homepage: www.elsevier.com/locate/bios

Enhanced photoelectrochemical biosensing performances for graphene (2D) – Titanium dioxide nanowire (1D) heterojunction polymer conductive nanosponges

N. Muthuchamy [a,1], K-P. Lee [a,b,c,1], A-I Gopalan [b,c,*]

[a] Department of Chemistry Education, Kyungpook National University, Daegu, South Korea
[b] Research Institute of Advanced Energy Technology, Kyungpook National University, Daegu, South Korea
[c] Department of Nanoscience and Nanotechnology, Kyungpook National University, Daegu, South Korea

ARTICLE INFO

Article history:
Received 21 April 2016
Received in revised form
3 June 2016
Accepted 3 June 2016

Keywords:
Graphene
Polymer nanosponge
Immobilization
Photoelectrochemical
Nitrite biosensing

ABSTRACT

In this work, an efficient photoelectrochemical (PEC) biosensing platform has been designed and developed based on graphene (G) through modifying it into an electroconductive polymer nanosponge (EPNS) and with the incorporation of titanium dioxide nanowires (TiO2 NW) (designated as TiO2 (G) NW@EPNS). Functioning as an efficient immobilization matrix for immobilization of the enzyme Cytochrome C (Cyt C), TiO2 (G) NW@EPNS delivers features for an efficient PEC biosensor, such as fast kinetics of direct electron transfer (DET) to the electrode and effective separation of photogenerated holes and electrons. TiO_2 (G) NW@EPNS exhibited DET to the electrode with a highly heterogeneous electron transfer rate constant of $6.29 \pm 0.002\ s^{-1}$. The existence of TiO_2, G and EPNS in conjunction facilitates DET between the electrode surface and the protein. The fabricated PEC nitrite ion (NO_2^-) biosensor showed superior analytical performances such as wide linear range (0.5–9000 μM), lowest detection limit (0.225 mM) and excellent specificity for NO_2^- in the presence other interferences at a very low bias potential (−0.11 V). This study opens up the feasibility of fabricating a PEC biosensor for any analyte using a matrix comprising of G and a photoactive material and EPNS, because these components synergistically contribute to effective immobilization of on enzyme, DET to the electrode and simple read-out under the light.

1. Introduction

The important sensor performances, such as good sensitivity and excellent selectivity towards analytes, of most of the enzyme-based biosensors, are greatly improved through the design and development of suitable biosensing matrices for effective immobilization of the enzyme (Wang et al., 2003). Likewise, establishing direct electron transfer (DET) between the immobilized enzyme and electrode surface is of great significance to fabricate advanced biosensors (Noll and Noll., 2011; Zheng et al., 2011). The establishment of DET not only obviates the troubles linked to the usage of special reagents (such as a mediator) in biosensors, but also offers the feasibility toward the fabrication of mediator free third-generation biosensors (Xu et al., 2006). The factors such as the unfavorable spatial orientation of enzyme at the support matrix, the proximity of active centers of the enzyme beyond the tunneling distance, denaturation of the enzyme by the substrate material and slow electron transfer kinetics at the substrate are responsible for hindering DET process at the electrode (Léger and Bertrand 2008). However, DET of proteins is rarely observed on bare electrodes mostly because of the burial of redox centers of the enzyme within the insulating protein shell. As a consequence of entrapment of redox sites, the spacing between the prosthetic group of the enzyme and the electrode surface exceeds the critical electron tunneling distance (Ronkainen et al., 2010). Strategies to maximize DET between the redox enzyme and electrode include the immobilization of an enzyme on an electroconductive and biocompatible surface. Also, the design of such enzyme electrode for effective DET should consider the factors to preserve both the protein structure and its native environment. The stringent requirements for achieving DET can be met through immobilization of the enzyme into a soft support matrix which can avoid enzyme denaturation. Over the past decades, the exploration of nanostructured materials has fueled research on the immobilization of biomolecules and the construction of DET based biosensors (Kandimalla et al., 2006). Various nanomaterials, which include nanostructured conducting polymers (Guo and Li., 2010), and

* Corresponding author at: Research Institute of Advanced Energy Technology, Kyungpook National University, Daegu, South Korea.
E-mail address: algopal_99@yahoo.com (AI. Gopalan).
[1] Authors contributed equally.

http://dx.doi.org/10.1016/j.bios.2016.06.005
0956-5663/

nanostructure metal oxides (Peng et al., 2011; Zhu et al., 2011), have shown the characteristics for establishing DET at the electrode. However, it remains a big challenge in developing new functional nanostructured materials comprising a soft polymer that can demonstrate the combined features such as fast DET capability, precise specificity toward the analyte, high sensitivity, and superior bioelectrocatalysis.

Two-dimensional (2D) nanomaterials, such as graphene (G), can function as excellent signal transducer elements in sensing devices due to their interesting physical and chemical characteristics (Chen et al., 2012; Chung et al., 2013; Loh et al., 2010; Gnach et al., 2015). However, the 2D nanomaterials should have adequate the cyto and biocompatibility characteristics for utilizing them in biosensing applications. The composition of 2D nanomaterials obviously determines the biocompatibility and other suitable features for biosensing applications. A literature search reveals that there is a rising interest in introducing biocompatibility to 2D nanomaterials toward using them in biosensor applications. Reports on the development of biocompatible 3D nanostructures from simple 2D nanomaterials are scarce. Notably, most of the previous researches were focused on transforming 2D G into 3D G based foams. Few studies have been focused on the development of the hydrogel/aerogel structures from G based 2D materials (Novoselov et al., 2004; Geim and Novoselov 2007; Allen et al., 2009; Han et al., 2013). Specifically, there is increasing interest in developing soft 3D nanomaterials from 2D G with the objective of using them in biomedical or biosensing applications. To our knowledge, the research on developing soft, hybrid and biocompatible 3D nanoarchitectures from 2D G has not been reported thus far.

Polymeric nanosponges (PNS) contain 3D polymer interconnected network structures having few-nanometer scale cavities or pores. The immobilization of enzymes into PNS is attractive for utilizing the inherent advantages of free enzymes, such as high catalytic power, and good selectivity for an analyte. PNS have intrinsic properties that are different from those of micro or macrosize supports, which make them ideal candidates for the development of nanobiocatalysts (Lin et al., 2012). The property profile of the immobilized enzyme is dependent on many factors such as the structure and properties of the PNS and the mode of enzyme immobilization into PNS (Ge et al., 2011). The encapsulation of an enzyme in a hydrophilic PNS ensures retention of water and provides adequate molecular conformation for the enzyme catalytic sites. These characteristics result in enhanced catalytic activities and stability of the enzyme (Yan et al., 2006). Also, electrical conductivity can be included to the insulating PNS through proper synthetic design strategies. Such novel electroconductive PNS (EPNS) can have highly interesting properties for a range of applications, e.g. electrodes in fuel cells, enzyme immobilization matrix in biosensors and bioelectrocatalysis. In this work, we developed an innovative and biocompatible EPNS comprising of interconnected polymer networks, 2D G and the one-dimensional (1D) titanium dioxide (TiO_2) nanowires (NW), toward fabricating a high-performance enzyme based photoelectrochemical (PEC) biosensor.

TiO_2 based semiconductor nanostructures have been shown to be potential electrode materials and good enzyme/biomolecule immobilization matrices because of their biocompatibility, relative conductivity, chemical and thermal stability (Doong and Shih 2006; Kafi et al., 2008). The electrochemical properties of TiO_2-based devices are not only influenced by the crystalline form of the TiO_2 but also likely affected by the textural properties of the TiO_2 such as dimension, geometry, porosity, and surface area. (Chen and Mao, 2007). Besides, the quantum confinement effect and electron transfer properties are mostly governed by the size and geometry of nanostructured TiO_2 (Burda et al., 2005). A high surface area and adequate pore distributions are especially beneficial for the fabrication of TiO_2 based bioelectronic devices, because these properties promote the interaction between biomolecules and TiO_2 as well provides high accessibility for the target analyte to the device surface.

PEC sensing represents a unique signal transducing modality involving separate processes for signal generation (photo) and detection (electrochemical) (Chen et al., 2010a; Tokudome et al., 2005). PEC sensors exhibit the striking advantages such as low background signals, high sensitivity, inherent miniaturization, portability and easy automation. Among the photocatalytic materials, TiO_2 has been widely utilized in the fabrication of PEC sensors due to its several beneficial features (Fujishima, 1972). One of the important issues in TiO_2 based PEC sensors is the selectivity toward a specific analyte. The composites of photoactive materials with enzymes (Gong et al., 2012) or molecularly imprinted polymers (Li et al., 2013; Wang et al., 2013) are considered to have enhanced selectivity for target species.

In this study, a novel PEC biosensor protocol was developed based on the in situ generated biocompatible EPNS on the surface of G embedded TiO_2(G) NW. We also demonstrated the fabrication of a PEC biosensor through immobilization of a redox protein, Cyt C. We report a simple method for the preparation of EPNS on the surface of TiO_2(G) NW to obtain TiO_2(G) NW@EPNS by utilizing the concept of "knitting" various polymeric chains through an appropriate cross-linker. We have chosen o-phenylene diamine (OPD) as the cross-linker to establish hyper cross-linking between poly (aniline) (PANI – an electroconductive polymer) and poly(acrylamido-2-propane sulfonic acid) (PAMPS – a biocompatible polymer). PAMPS has attracted wide applications as biomaterials and hemocompatible carrier (Nalampang et al., 2013; Bartlett et al., 2012). The cross-linking polymerization was performed in the presence of 2-vinylaniline (VA), 2-acrylamido-2-methyl-1-propanesulfonic acid (AMPS), aniline and TiO_2(G) NW and initiated by ammonium persulfate (APS) (Scheme-1). During the hyper cross-linking reaction to form EPNS, poly (OPD) chains serve as the bridges to establish cross-links with chains of other polymers, PAMPS, and PANI. The TiO_2(G) NW@EPNS/Cyt C based PEC biosensor was fabricated with immobilization of Cyt C into TiO_2(G) NW@EPNS. The newly prepared TiO_2(G) NW@EPNS/Cyt C generates photoelectrons under light irradiation and consequently results in PEC current responses for nitrite ions (NO_2^-) at a low potential (−0.11 V). Thus, a low-potential PEC biosensing of NO_2^- has been demonstrated. The proposed PEC biosensor showed good performances, such as rapid response time (~5 s), wide concentration range (0.5 mM to 9 mM), good selectivity and a low applied potential (−0.11 V) toward monitoring the concentration of NO_2^-.

2. Experimental

2.1. Chemicals

The materials utilized in this work are listed in supporting information-1(SI-1).

2.1.1. Preparation of TiO_2(G) NW@EPNS

G was carboxylated (G-COOH) (SI-2) and included within the TiO_2(G) NW through combined electrospinning-hydrothermal process (Lee et al., 2015a). About 40 mg of TiO_2(G) NW was well dispersed in 45 mL of 0.1 M HCl for 30 min. Then, aniline (20 mM), OPD (10 mM), AMPS (50 mM) and 5 mM of VA were added to the above dispersion at 5 °C. After about 30 min of stirring, 5 mL of 0.1 M APS solution was added dropwise and kept for 6 h in the stirred condition. Finally, the as-prepared sample (TiO_2(G)

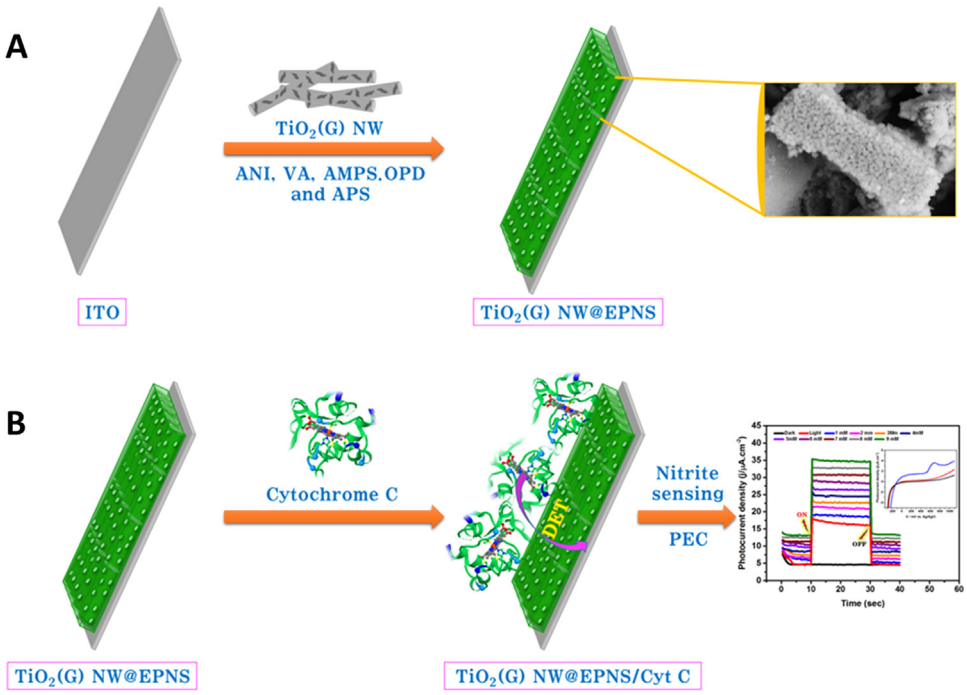

Scheme 1. (A) Preparation of electroconductive polymer nanosponges coated TiO_2(G) (TiO_2(G) NW@EPNS) and (B) immobilization of cytochrome c (Cyt C) to fabricate TiO_2(G) NW@EPNS/Cyt C biosensor and photo amperometric biosensing.

NW@EPNS) was repeatedly washed with 0.1 M HCl (till the filtrate was colorless) and dried at 60 °C for 8 h. For comparative purposes, TiO_2 NW@EPNS and pristine EPNS were also prepared using pristine TiO_2-NWs and in the absence of TiO_2(G) NWs, respectively.

2.1.2. *Fabrication of TiO_2(G) NW@EPNS/Cyt C biosensor*

About 10 mg of TiO_2(G) NW@EPNS was dispersed in 1:3 (v/v) of 5% Nafion and isopropyl alcohol (total 0.12 mL) under sonication. About 6 μL of the above dispersion was dropped onto the surface of the indium tin oxide (ITO) surface (area = 0.25 cm^2) and dried in air. The modified electrode, ITO/TiO_2(G) NW@EPNS (hereafter mentioned as TiO_2(G) NW@EPNS) was immersed in 0.1 M PBS (pH 6.8) solution containing 1 mg/mL Cyt C for 10 min. In the final step of the TiO_2(G), NW@EPNS/Cyt C biosensor was removed from the Cyt C solution and washed three times with distilled water (to remove the loose adsorbed Cyt C). Similarly, TiO_2 NW@EPNS/Cyt C and EPNS/Cyt C biosensors were also fabricated.

2.2. *Instrumentation*

All electrochemical experiments were performed at an IVIUMSTAT and COMPACTSTAT (The Netherlands) electrochemical workstation. The morphology of the synthesized materials was observed by field-emission scanning electron microscopy (FE-SEM, S-4300, Hitachi, Japan) and field-emission transmission electron microscope (FE-TEM, 200KV, DS114). Fourier transform infrared (FTIR) spectra were recorded (1486.6 eV) on a Bomem MB 100 FT-IR spectrometer (ABB Bomem, QC, Canada) in the wavenumber range between 400 and 4000 cm^{-1}.

2.3. *Electrochemical experiments and PEC sensing*

Typically, a conventional three electrode cell set-up comprising of ITO modified TiO_2(G) NW@EPNS/Cyt C (working), a platinum wire (counter), and an Ag/AgCl (reference) electrode, was used for the electrochemical measurements. Electrochemical impedance spectroscopy (EIS) measurements were performed in an aqueous solution containing equimolar of $K_3Fe(CN)_6/K_4Fe(CN)_6$ (5 mM) in the frequency range of 100 kHz - 0.01 Hz. The PEC measurements were carried out by irradiation of working electrode with a UV lamp (Viller Lourmat, France, 365 nm (4 W) placed at a distance of 10 cm. The NO_2^- biosensing measurements were done in an electrochemical cell by immersing the TiO_2(G) NW@EPNS/Cyt C biosensor in 0.1 M PBS (pH = 7.0) solution under light irradiation or dark for different concentrations of NO_2^-.

3. Result and discussion

3.1. *Synthesis and characteristics of TiO_2(G) NW@EPNS*

We modified 2D G into a new biocompatible 3D EPNS for using in PEC biosensing application. The newly synthesized PEC sensing material, TiO_2(G) NW@EPNS, includes the photocatalytic TiO_2 NW, 2D G, and electron transfer-mediating EPNS. The results showed that the components, TiO_2(G) NW and EPNS, synergistically improved the photocatalytic, electron transfer and biocompatibility properties. We designed the synthesis of TiO_2(G) NW@EPNS through a simple room temperature cross-linking polymerization to generate hyper-cross-linked networks between PANI and PAMPS via the POPD bridges in the presence of pre-synthesized TiO_2(G) NW. The structural aspects of TiO_2(G) NW@EPNS, as derived from FTIR spectroscopy, are detailed in SI3. Typically, FTIR spectra of TiO_2(G) NW@EPNS, TiO_2 NW@EPNS and pristine EPNS (Fig. SI3) revealed the prominent existences of imine (=N–) and amine (–NH–) groups as well the cross-linked structures established through phenazine bridges.

The morphologies and microstructures of TiO_2(G) NW@EPNS and other synthesized samples were investigated by the FE-SEM and TEM images in Fig. 1 and SI4. A close comparison of the FE-SEM images of TiO_2(G) NW@EPNS (Fig. 1A) and pristine TiO_2(G) NW (Fig. 1A) revealed the morphological variations between them. FE-SEM image of TiO_2(G) NW@EPNS (Fig. 1A) shows the existence

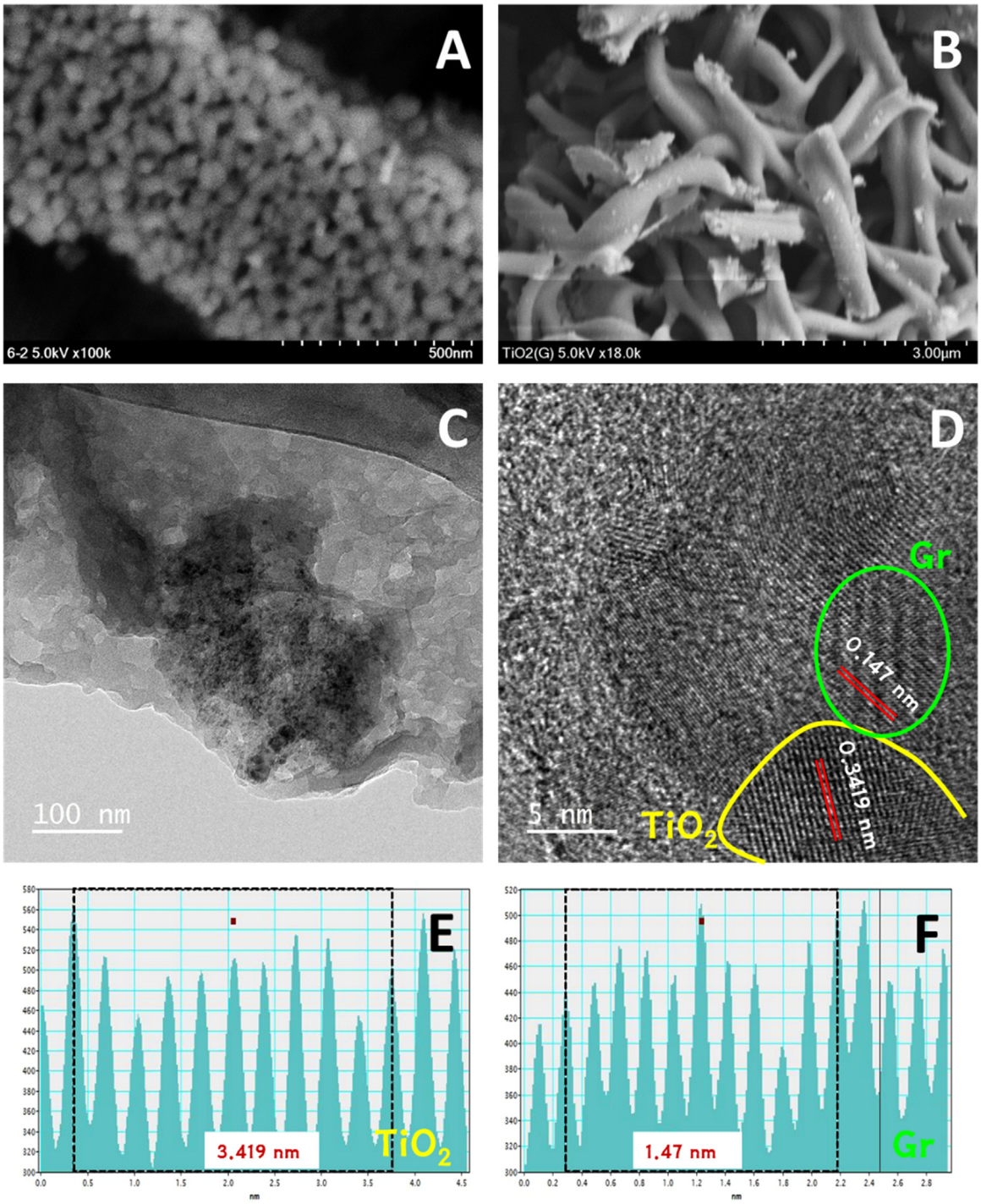

Fig. 1. FE-SEM image of **(A)** TiO_2(G) NW@EPNS, **(B)** pristine TiO_2 NW, **(C)** FE-TEM image of TiO_2(G) NW@EPNS; **(D)** and a higher magnification FE-TEM image of TiO_2(G) NW@EPNS. Interplanar distances and intensities of 10 diffraction peaks of **(E)** TiO_2 and **(F)** G.

3D porous frameworks originated through the agglomeration of spherical polymer particles (sizes ranging from 10 to 35 nm in diameters). On the contrary, FE-SEM image of pristine TiO_2(G) NW (Fig. 1B) informs the presence of interconnected nanowires having diameters in the range from 195 to 270 nm and lengths of several micrometers. FE-SEM image of TiO_2(G) NW@EPNS (Fig. 1A) suggests that the wires of pristine TiO_2(G) NW (Fig. 1B) are fully covered by the polymer networks (EPNS). So, after the formation of EPNS, the wires of TiO_2(G) NW are transformed into a well-ordered rectangular block shaped NS. The typical FE-SEM image of TiO_2(G) NW@EPNS (Fig. 1A) reveals the dimensions; length, width and height of the rectangular block NS as 2 μM, ~370 nm and ~40 nm, respectively. The 3D block rectangular NS is expected to be generated through the 2D G guided growth. The roles of G in guiding the 3D nanomorphology of materials have earlier been detailed (Williams et al., 2008; Xu et al., 2015; Li et al., 2015). On comparison of the FE-SEM images of the TiO_2 NW@EPNS (Fig. SI4 A) and pristine EPNS (Fig. SI4 B) with the image of TiO_2(G) NW@EPNS (Fig. 1A), can can notice NS type morphology only for TiO_2(G) NW@EPNS (Fig. 1A). In the present case, the TiO_2(G) NW@EPNS consists of three main phases, TiO_2 NWs, dispersed G sheets and a polymer phase (EPNS). However, FE-SEM image of

Please cite this article as: Muthuchamy, N., et al., Biosensors and Bioelectronics (2016), http://dx.doi.org/10.1016/j.bios.2016.06.005

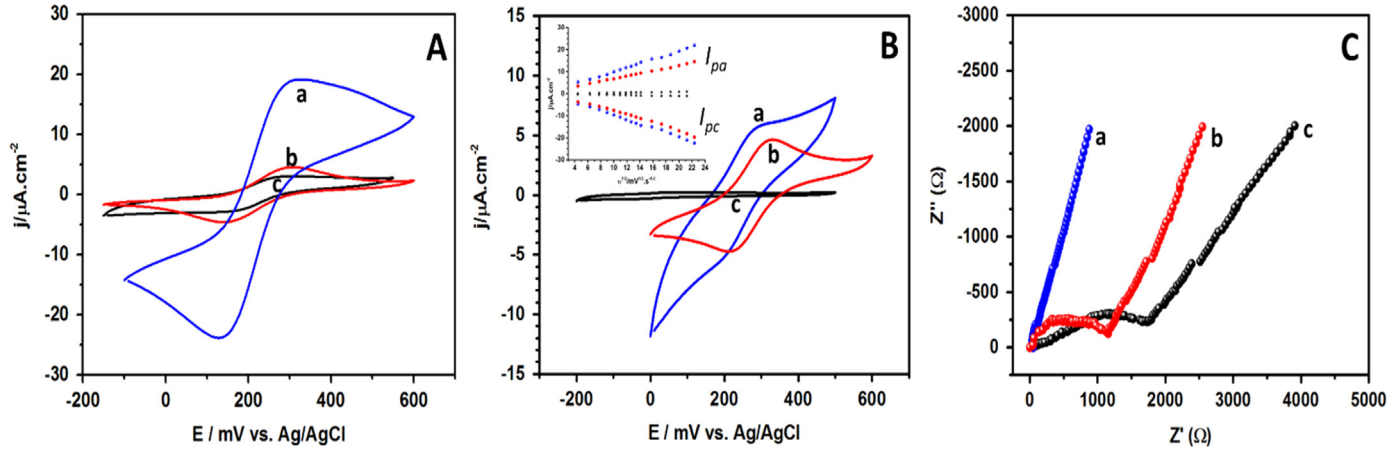

Fig. 2. (A) Cyclic voltammograms of (a) TiO_2(G) NW@EPNS (b) TiO_2 NW@EPNS and (c) pristine EPNS in 0.1 M KCl containing 5 mM of $Fe(CN)_6^{3-/4-}$ at the scan rate of 50 mV s^{-1}. **(B)** Cyclic voltammograms and **(C)** Nyquist plots of (a) TiO_2(G) NW@EPNS/Cyt C, (b) TiO_2 NW@EPNS/Cyt C, and (c) EPNS/Cyt C. **Inset (B):** Linear plot of square root of scan rate ($\upsilon^{1/2}$) *Vs* peak current (I_p) and **(C)** (a) EIS spectra of TiO_2(G) NW@EPNS (b) TiO_2 NW@EPNS and (c) pristine EPNS in the frequency range of 100 kHz–0.01 Hz.

TiO_2(G) NW@EPNS (Fig. 1A) does not provide the subtitle details of the individual components. The TEM image in Fig. 1C shows that TiO_2 NW and G nanofillers are embedded in the polymer matrix (EPNS) with sufficient interconnections. And, the TEM image at a higher magnification (Fig. 1D) clearly reveals that TiO_2(G) NW@EPNS comprises of an amorphous (polymer) phase and two (TiO_2 and (G)) crystalline regions, with an interplanar spacing of 0.342 nm (Sasaki and Watanabe, 1997) (average of 10 interplanar distances (Fig. 1E)) that corresponds to (101) atomic plane of anatase TiO_2 and an interplanar distance of 0.147 nm (average of 10 interplanar distances (Fig. 1F)), that is attributed to the atomic distance of hexagonal atomic lattice in G (Wilson et al., 2009; Geim and Novoselov, 2007).

3.2. Electrochemical characteristics

Cyclic voltammograms (CVs) of (a) TiO_2(G) NW@EPNS, (b) TiO_2 NW@EPNS, and (c) pristine EPNS electrodes, were recorded in 0.1 M KCl containing 5 mM of $Fe(CN)_6^{3-/4-}$ each at the scan rate (υ) of 50 mV s^{-1} (Fig. 2A). CVs exhibited a pair of electrochemical peaks that corresponded to the $Fe(CN)_6^{3-/4-}$ redox process and suggested the occurrence of reversible reactions at the electrode surface. Typically, the TiO_2(G) NW@EPNS electrode (Fig. 2A(curve a)) showed about 4.2 and 6.2 times the higher anodic peak current than that of the peak currents of TiO_2 NW@EPNS (Fig. 2A(curve b)) and pristine EPNS (Fig. 2A(curve c)) electrodes. The larger peak current for TiO_2(G) NW@EPNS suggests that the electron transfer process is facilitated at TiO_2(G) NW@EPNS electrode as compared to TiO_2 NW and pristine EPNS electrodes. The highest peak current noticed for TiO_2(G) NW@EPNS electrode is ascribed to the good adsorption of the redox probe by the porous EPNS and conductive nature of TiO_2(G) NW. We also compared the CVs of TiO_2(G) NW@EPNS, TiO_2 NW@EPNS, and pristine EPNS electrodes after immobilization of similar amounts of Cyt C (Fig. 2. B). CVs of TiO_2(G) NW@EPNS/Cyt C (Fig. 2B(curve a)), TiO_2 NW@EPNS/Cyt C (Fig. 2B(curve b)), and pristine EPNS/Cyt C (Fig. 2B(curve c)) electrodes exhibited higher peak currents for the $Fe(CN)_6^{3-/4-}$ redox process as compared to the peak currents of TiO_2(G) NW@EPNS (Fig. 2A(curve a)), TiO_2 NW@EPNS (Fig. 2A(curve b)) and pristine EPNS (Fig. 2A(curve c)) electrodes. The above results suggest two information. Firstly, the $Fe(CN)_6^{3-/4-}$ electron transfer process is facilitated at Cyt C immobilized electrodes as the electrons can be shuttled via the $Fe^{(II)}/Fe^{(III)}$ redox sites in heme protein of Cyt C. Secondly, the electroactivity of the electrode is not blocked by the immobilized of Cyt C proteins. In the case of pristine EPNS/Cyt C electrode, the peak currents were deplorably low (Fig. 2B(curve c)) as compared to that of TiO_2(G) NW@EPNS/Cyt C (Fig. 2B(curve a)), TiO_2 NW@EPNS/Cyt C (Fig. 2B(curve b)) electrodes. The larger electroactive surface area of the electrode due to the inclusions of TiO_2 NW and TiO_2(G) NW contributes to the increase in currents. SI. 5 presents the CVs of TiO_2(G) NW@EPNS/Cyt C (Fig. 2B(curve a)), TiO_2 NW@EPNS/Cyt C (Fig. 2B (curve b)) and EPNS/Cyt C electrode, recorded at various υ. The electroactive surface area (A) (SI 5) of TiO_2(G) NW@EPNS/Cyt C electrode was derived from the plot of peak current vs υ (Fig. 2B (inset)) and found to be ~2.85 and ~4.77 times higher than the A of TiO_2 NW@EPNS/Cyt C and EPNS/Cyt C, respectively. The results ensured that TiO_2(G) NW@EPNS/Cyt C possesses the highest A value as compared to rest of the fabricated electrodes in this study.

EIS measurements were carried out to investigate the surface electron transfer properties of the modified electrodes. SI 6 describes the typical Nyquist plots of different modified electrodes, TiO_2(G) NW@EPNS, TiO_2 NW@EPNS and pristine EPNS. The electron transfer resistance (R_{ct}) of the electrodes takes the order: TiO_2(G) NW@EPNS (320Ω) < TiO_2 NW@EPNS (670Ω) < pristine EPNS (1050Ω) (SI 6). The smallest R_{ct} for TiO_2(G) NW@EPNS (320Ω) suggests that G in the electrode surface augments the electron transfer process. The R_{ct} values for the three electrodes, TiO_2(G) NW@EPNS/Cyt C, TiO_2 NW@EPNS/Cyt C, and pristine EPNS/Cyt C (Fig. 2C) are lower as compared to electrodes without Cyt C immobilization. The electron transfer is expected to be rmediated through the heme protein, Cyt C, via the Cyt C (Fe^{3+})+ Fe^{2+} ⇌ Cyt C (Fe^{3+})–Fe^{2+} ⇌Cyt C(Fe^{2+})–Fe^{3+} reactions (Ohno and Cusanovich, 1981).

3.3. Direct electrochemistry of TiO_2(G) NW@EPNS/Cyt C electrode

We used cyclic voltammetry to evaluate the electrochemical characteristics of the immobilized Cyt C molecules on the modified electrodes. Fig. 3. A shows the typical CVs of TiO_2(G) NW@EPNS/Cyt C, TiO_2 NW@EPNS/Cyt C, ECNS/Cyt C and TiO_2(G) NW@EPNS electrodes in 0.1 M PBS (pH 6.8) at a scan rate of 50 mV s^{-1}. CVs of TiO_2(G) NW@EPNS/Cyt C (curve a) show a pair of well-defined redox peaks (E_{pa} at −0.11 V and E_{pc} at −0.19 V vs. Ag/AgCl) which correspond to Fe(II)/Fe(III) electronic transitions in Cyt. These electrochemical features are assigned to one electron quasi-reversible redox process of Cyt C. The formal potential (E^o) of Cyt C redox process ($E^o_{Cyt\,C}$), −0.15 V is close to the reported value of −0.147 V for native Cyt C (Yamamoto et al., 2001). Thus, the existence of DET of the heme protein at TiO_2(G) NW@EPNS/Cyt C

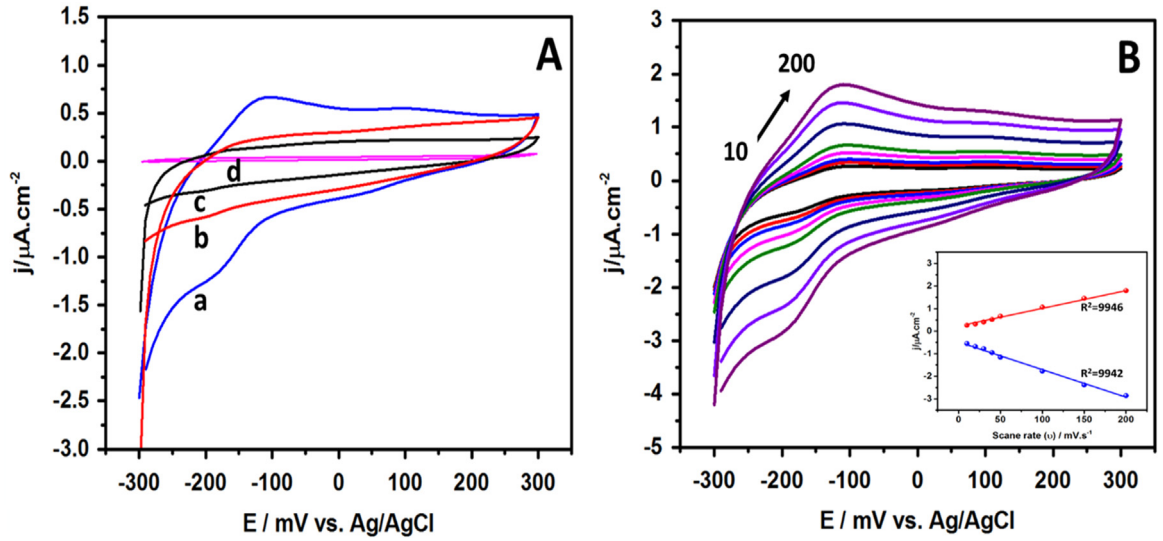

Fig. 3. (A) Cyclic voltammograms of (a) TiO_2(G) NW@EPNS/Cyt C, (b) TiO_2NW@EPNS/Cyt C, (c) EPNS/Cyt Cand (d) TiO_2(G) NW@EPNS electrodes in 0.1 M PBS (pH 6.8) at a scan rate of 50 mV s^{-1}; **(B)** Cyclic voltammograms of TiO_2(G) NW@EPNS/Cyt C recorded for various scan rates (10, 20, 30, 40, 50, 100, 150, and 200 mV s^{-1}). **Inset (B)** Linear plots of anodic and cathodic peak current *Vs.* scan rate.

electrode is confirmed. Similar, direct and un-mediated electrochemistry has been earlier witnessed for Cyt C at the surface of various modified electrodes (Dinesh et al., 2014; Wang et al., 2002; Lee et al., 2009).

Cyt C is a basic protein and can have interactions with negatively charged sites on the immobilization matrix through its charged lysine residues (Moretto et al., 2005). Nevertheless, the minimum shift noticed in $E^{o}_{Cyt\,C}$ as compared to $E^{o}_{Cyt\,C}$ of the native protein indicates that interactions between the surface ligands in Cyt C and materials in TiO_2(G) NW@EPNS/Cyt C electrode are negligible (Khoshtariya et al., 2003). The electrochemical features in Fig. 3A (curve a) are in accordance with the native configuration of the immobilized Cyt C at TiO_2(G) NW@EPNS/Cyt C electrode without having interactions with the surrounding environments. The EPNS in the immobilization matrix of TiO_2(G) NW@EPNS/Cyt C comprises of PMPA, a hydrophilic polymer containing SO_3H groups and the cross-linked networks of PANI chains having protonated amine (–NH^+–) and imine (=N^+–) groups. The PMPA and PANI chains are knitted through cross-links, and their electrical charges are nearly compensated. Hence, the nearly neutral EPNS (pH ~6.8) serves as a non-interactive matrix for the immobilized Cyt C. The non-interactive EPNS provides a favorable microenvironment for the Cytc to retain its native environment. In its native configuration, the thioether bonds of Cyt C ensure that the heme prosthetic groups are closely associated. Also, the heme groups are axially linked through the histidine and methionine side chains. In the absence of interactions with exogenous groups, the methionine-iron bond is undisturbed. Such a native configuration contributes to the quasi-reversible redox property of Cyt C (Dobson et al., 1998). In this work, Cyt C displays a well-defined quasi-revers electrochemistry at TiO_2(G) NW@EPNS/Cyt C matrix, as similar to the earlier reports on Cyt C immobilized polymeric Langmuir-Blodgett thin-film (Liu et al., 2001; Moretto et al., 2005). The following factors contribute to DET at TiO_2(G) NW@EPNS electrode; distance between the redox center of Cyt C and electrode surface, increase in the effective surface area of the modified electrode, increase in electrical conductivity and biocompatible microenvironment for Cyt C. Also, CVs of TiO_2 NW@EPNS/Cyt C (Fig. 3A (curve b)) and ECNS/Cyt C (Fig. 3A(curve c)) did not show the DET electrochemical features of Cyt C. For ascertaining the role of Cyt C on the electrochemical features at TiO_2(G) NW@EPNS electrode, we recorded the CV of TiO_2(G) NW@EPNS electrode (without Cyt C immobilization) (Fig. 3A(curve d)). The CV of TiO_2(G) NW@EPNS electrode did not show any prominent redox peaks in the potential window (-0.3 to $+0.3$ V).

We recorded the CVs of the TiO_2(G) NW@EPNS/Cyt C electrode for various υ in PBS (pH 6.8) to investigate the effect of scan rate (γ) on the voltammetric behavior of Cyt C (Fig. 3B). Both cathodic and anodic peak currents of the redox transitions of Cyt C increased linearly with increase in υ (Fig. 3B (inset)), which suggested the occurrence of surface confined quasi-reversible process at the TiO_2(G) NW@EPNS/Cyt C electrode (Cao et al., 2008). The electron transfer rate constant for DET of Cyt C (k_s (Cyt C)) at TiO_2(G) NW@EPNS/Cyt C was calculated as $6.29 \pm 0.0023\ s^{-1}$, based on Laviron (R) model for a surface control electrode process. The value of k_s(Cyt C) is much higher at TiO_2(G) NW@EPNS/Cyt C than that reported for various other Cyt C immobilized modified electrodes (Geng et al., 2008; Koh et al., 2008; Chen et al., 2009; Eguilaz et al., 2010; Zhu et al., 2009). Also, the values of surface excess concentration of Cyt C (Γ, mol cm^{-2}) were calculated as 4.59×10^{-10} mol cm^{-2}, 8.51×10^{-11} mol cm^{-2} and 1.5×10^{-11} mol cm^{-2}, for the modified electrodes, TiO_2(G) NW@EPNS/Cyt C, TiO_2 NW@EPNS/Cyt C and EPNS/Cyt C, respectively. The Γ of Cyt C at TiO_2(G) NW@EPNS/Cyt C (4.59×10^{-10} mol cm^{-2}) is much higher than the theoretical value of monolayer coverage (1.40×10^{-12} mol cm^{-2}) (Dickerson et al., 1971) and Γ of other modified electrodes, such as Cyt c/L-Cys/P3MT/MWCNT/GCE and MWCNTs–DNA–cyt c (Eguilaz et al., 2010; Shie et al., 2008; Gopalan et al., 2010), The high Γ of Cyt C at TiO_2(G) NW@EPNS originates from the large surface area and excellent loading of Cyt C.

The stability of Cyt C within the TiO_2(G) NW@EPNS matrix was tested by keeping the Cyt C immobilized electrode in 0.1 M PBS for a period 7 days. The UV–visible spectrum of the PBS solution (in which TiO_2(G) NW@EPNS/Cyt C electrode was kept) was periodically recorded. The UV–visible spectrum of the PBS solution did not exhibit any of the spectral features of Cyt C. This is ascertained from the electronic spectrum of Cyt C in PBS (0.1 M). The electronic absorption spectrum of Cyt C displays a soret band at 415 nm and two Q bands at 520 nm and 550 nm, respectively (Margoliash et al., 1959). The absence of the spectral characteristics of Cyt C in the PBS solution (in which TiO_2(G) NW@EPNS/Cyt C electrode was kept) signified that Cyt C was stable at the TiO_2(G) NW@EPNS matrix without leaching into PBS solution. Also, after keeping the TiO_2(G) NW@EPNS/Cyt C electrode in 0.1 m BPS solution for 7 days, the electrode exhibited the redox peaks that corresponded

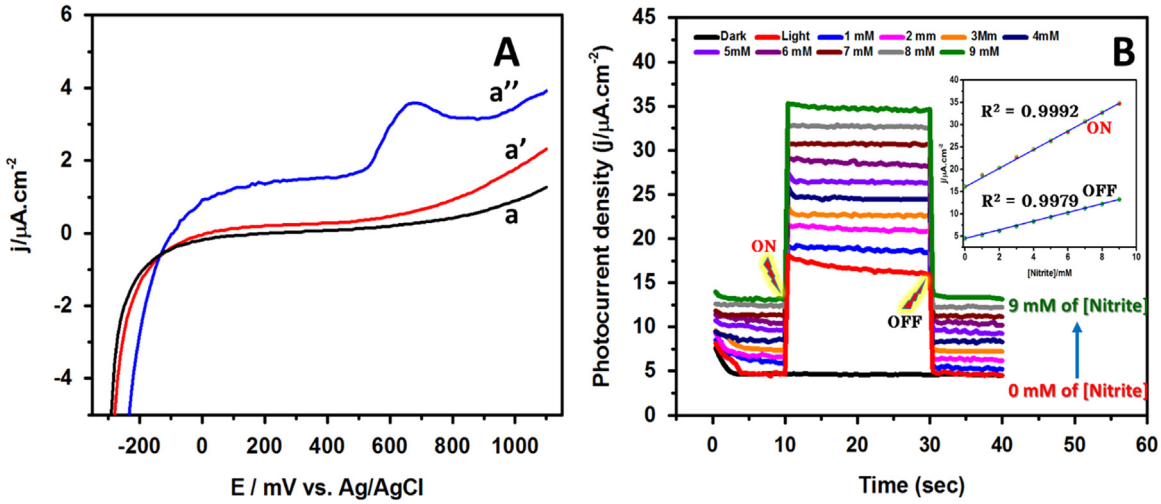

Fig. 4. (A) Linear sweep voltammograms of TiO_2(G) NW@EPNS/Cyt C biosensor in (a) dark, without NO_2^-; (a′) dark, with 1 mM NO_2^-; and (a") under light irradiation, with 1 mM NO_2^- in 0.1 M PBS (pH 6.8) at a scan rate 50 mV s^{-1}. **(B)** Photochronoamperometric responses of TiO_2(G) NW@EPNS/Cyt C biosensor (applied potential (E) = −0.11 V) for successive addition of NO_2^- concentrations. Inset: linear plot of concentration of NO_2^- *Vs* photocurrent.

to DET of Cyt C with an almost un-altered $E^o_{Cyt\,C}$ and redox peak currents. These features provide evidences that the immobilized Cyt C within TiO_2(G) NW@EPNS was stable and retained its electroactivities over the tested period of 7 days.

3.4. Photoelectrochemical performance of the TiO_2(G) NW@EPNS/Cyt C towards NO_2^- biosensor

Recently, we have independently reported the performances of two NO_2^- electrochemical biosensors; one based on immobilization of Cyt C into a 3D nano architectured electrode comprising of three components (TiO_2, G and thiol functionalized PANI) (Komathi et al., 2016) and the another involving immobilization of Cyt C into titanium nitrate/multiwall carbon nanotube composite (Haldorai et al., 2016). DET for Cyt C was witnessed in both the matrices. However, the reported NO_2^- biosensors (Komathi et al., 2016; Haldorai et al., 2016) were designed based on the electrocatalytic oxidation of NO_2^-. Hence, the electrochemical NO_2^- biosensing was performed by amperometry at a much higher positive potentials (+0.90 V (Komathi et al., 2016) and ~0.92 V (Haldorai et al., 2016)). Generally, the application of a high (~+0.90 V) potential for electrochemical biosensing of NO_2^- is expected to hinder the selectivity of the NO_2^- biosensors in the presence of common interfering ions and other organic interferences. Nevertheless, we obtained good selectivity for NO_2^- biosensing (Komathi et al., 2016; Haldorai et al., 2016) because of the relatively lower kinetics of charge transfer process of the inferents as compared to faster DET of Cyt C at those biosensing electrodes (Komathi et al., 2016; Haldorai et al., 2016). In the present work, the TiO_2(G) NW@EPNS/Cyt C biosensor for NO_2^- is superior and advantageous over the other two reports, in two specific aspects: firstly, we designed to utilize TiO_2(G) NW@EPNS/Cyt C as a PEC biosensing platform. Secondly, the biosensing of NO_2^- was achievable at a much lower applied potential (very close to the $E^o_{Cyt\,C}$). We applied a light irradiation to generate the photo electrons and followed the photocurrent at a very low applied potential (close to the $E^o_{Cyt\,C}$) through photoamperometry.

It is to be noted that pristine TiO_2 nanostructured materials having TiO_2 network exhibit inferior electrical conductivities and hence their electrochemical applications are hampered (JACS, 135, 9015 (2013)). However, compositing TiO_2 with conducting materials, such as G, nanostructured PANI or metal nanoparticles, can significantly enhance the electrochemical/catalytic properties of TiO_2 (Li et al., 2014a, 2014b; Qiao et al., 2007). Among the various TiO_2 based composites, TiO_2-G composite nanostructures are extensively used as advanced photo electrocatalysts (Qiu et al., 2014; Xiang et al., 2012). Typically, G in TiO_2-G composites enhances the conductivity of TiO_2 and allows the photogenerated electron to be transferred more efficiently due to its function as an electron acceptor. The TiO_2-G composites prepared by physical blendings are characterized to have weak interaction between TiO_2 and G. On the other hand, distribution of G sheets into TiO_2 networks via chemical bonds can improve the stability of composite as well promotes the charge separation and electron transport between TiO_2 and G (Mou et al., 2014). Likewise, the distribution of G within TiO_2 nanostructure prevents the G sheets from restacking, which is beneficial for the TiO_2-G composites for increasing the specific surface area. In our work, we used TiO_2(G) NW prepared through electrospinning (Lee et al., 2015a). Our results clearly documented that G sheets were distributed within TiO_2 NW and Ti–O–C bonds were established (Lee et al., 2015b). Thus, our purpose to utilize TiO_2(G) NW@EPNS as a porous and photoactive 3D matrix (Fig. 1A) for the PEC biosensing of NO_2^- is justified.

For the purpose of evaluating the photocatalytic properties of TiO_2(G) NW@EPNS/Cyt C electrode, linear sweep voltammograms (LSVs) were firstly collected in the absence and presence of 1 mM of NO_2^- in aqueous PBS (0.1 M, pH = 6.8) solution under dark and light irradiation conditions. Under the light irradiation condition, the LSV of 1 mM NO_2^- containing solution showed a sharp increase in peak currents starting from −0.11 V and a prominent peak at +0.75 V (Fig. 4A(curve a")). It is obvious that TiO_2(G) NW is the photoresponsive component to cause the photocurrent. To confirm the role of TiO_2(G) NW toward photocurrent generation, LSV was recorded for TiO_2(G) NW@EPNS/Cyt C in the absence of light (dark condition, Fig. 4A(curve a')). The CV showed deplorably low currents in the potential range from −0.11 V to +0.80 V for TiO_2(G) NW@EPNS/Cyt C under dark (Fig. 4A(curve a)). The two electrodes, TiO_2 NW@EPNS/Cyt C and EPNS/Cyt C did not show any electrochemical features in the potential window (from −0.20 V to +1.20 V) in the presence of NO_2^- under both in dark as well in light irradiation conditions. Thus, the photocurrent generated at the TiO_2(G) NW@EPNS/Cyt C electrode can be applied as the analytical signal for the detection of NO_2^-. We performed NO_2^- PEC biosensor experiments with optimized conditions such as pH = 6.8 (SI 7) and a loading of 10 mg mL^{-1} (SI 8).

3.4.1. PEC determination of NO_2^-

We evaluated the PEC responses of TiO_2(G) NW@EPNS/Cyt C

biosensor as a function of NO_2^- concentration through photoamperometric experiments. The PEC responses were evaluated at a fixed potential at (−0.11 V) under light on/off cycles (Fig. 4B). The response time for PEC NO_2^- sensing was estimated as ~5 s from the time taken for reaching 94% of the photocurrent at −0.11 V. As shown in the inset of Fig. 4B, the sequential addition of NO_2^- concentration increases the photocurrent at −0.11 V in the range from 0.5 to 9000 μM. The photocurrent was larger at TiO_2(G) NW@EPNS/Cyt C biosensor for any NO_2^- concentration (between 0.5–9000 μM) as compared to 'light off' conditions. The photocurrents showed a linear relation with a concentration of NO_2^- (Fig. 4. B(inset)) in the "light on" condition with the following equation.

$$I_{photo}(\mathrm{mA}) = 0.2018[NO_2^-]\mu\mathrm{M} + 0.0301 \quad (R^2 = 0.9992) \tag{1}$$

The limit of detection (LOD) for NO_2^- sensing was estimated as 0.225 μM (SI 9) in the "light on" condition under the signal to noise ratio of 3. The PEC performances of the TiO_2(G) NW@EPNS/Cyt C for NO_2^- sensing are compared with other the NO_2^- biosensors (Table 1). Notably, the majority of NO_2^- biosensors reported in literature utilized the electrochemical detection modes (amperometry, cyclic voltammetry and differential pulse voltammetry) to follow the electrocatalytic oxidation/reduction of NO_2^-. The PEC biosensing of NO_2^- at TiO_2(G) NW@EPNS/Cyt C, as described in this work, is superior in two aspects over the other NO_2^- biosensors reported in literature: Firstly, the PEC NO_2^- biosensing in this work, was performed at a much lower bias potential (−0.11 V) for the first time, which signifies the advantage of minimum interferences from the co-existing species. Secondly, we report a wide concentration range (0.5–9000 μM) for PEC NO_2^- detection in combination with the sensing NO_2^- at a very low potential. These special performances of NO_2^- biosensor at TiO_2(G) NW@EPNS/Cyt C are attributed to the synergistic influences of porous EPNS (Fig. 1A) and G embedded TiO_2 NW. The components, EPNS and TiO_2(G) NW, contribute the effective immobilization of Cyt C, DET of Cyt C and PEC sensing with good performances (Table 1).

We propose the following mechanism for the PEC biosensing of NO_2^- at TiO_2(G) NW@EPNS/Cyt C. The mechanism involves the initial excitation of TiO_2 by light to generate photoelectrons ($e^-_{(photo)}$). The photo excited electrons are transferred from the conducting band of TiO_2 to G due to the good electron accepting property of G (Lee et al., 2015a). The heme-Fe(III) sites in the immobilized Cyt C are transformed into heme-Fe(II) sites through interactions with $e^-_{(photo)}$ (Eq. (2))

$$CytC_{(heme-Fe(III))} + e^-_{(photo)} \rightarrow CytC_{(heme-Fe(II))} \tag{2}$$

It has earlier been proposed that it is not the NO_2^- but the nitric oxide (NO), generated by NO_2^- disproportionation reaction (Eq. (3)), directly interacts with the active sites of the heme-proteins (Younathan et al., 1992). The $Cyt\ C_{(heme-Fe(II))}$ sites (Eq. (2)) bind and eventually transform the NO to nitrous oxide (N_2O) (Eqs. (4) and (5))

$$3NO_2^- + H_2O \leftrightarrow 2NO + NO_3^- + 2OH^- \tag{3}$$

$$CytC_{(heme-Fe(II))} + NO \rightarrow CytC_{(heme-Fe(III))} - NO \tag{4}$$

$$CytC_{(heme-Fe(III))} - NO + 2e^- \overset{+H^+}{\rightarrow} CytC(heme-Fe(II)) + H_2O + N_2O \tag{5}$$

The application of low potential (−0.11 V), for the amperometric measurements, signifies the predominance of the reduction process, as described in Eq. (5) (Dai et al., 2004; Zhang et al., 2008; Ding et al., 2010).

3.5. Interference

We examined the influence of the ions such as Na^+, K^+, NH_4^+, Mg^{2+}, Ca^{2+}, Zn^{2+}, Al^{3+}, Cl^-, ClO_4^-, NO_3^-, SO_3^-, $H_2PO_4^-$, SO_4^{2-}, HPO_4^{2-}, PO_4^{3-} H_2O_2 and organic molecules such as uric acid, methanol, and glucose on the photocurrent response of NO_2^- (1 mM) at TiO_2(G) NW@EPNS/Cyt C biosensor. The photocurrent measurements were independently done for solutions containing a fixed amount of NO_2^- (1 mM) and 50-fold excess concentration of Na^+, K^+, NH_4^+, Mg^{2+}, Ca^{2+}, Zn^{2+}, Al^{3+}, Cl^-, ClO_4^-, NO_3^-, SO_3^-, $H_2PO_4^-$, SO_4^{2-}, HPO_4^{2-}, PO_4^{3-}. Likewise, experiments were done with a 10-fold excess concentration of H_2O_2, uric acid, methanol, and glucose. There was no interference for NO_2^- sensing in the presence of these foreign species. The results demonstrated that TiO_2(G) NW@EPNS/Cyt C biosensor exhibits good selectivity for NO_2^-. The salient reason for the selectivity toward NO_2^- is the very low bias potential (−0.11 V) and the PEC mode for the signals.

Table 1
Comparison of the analytical performances between TiO_2(G) NW@EPNS/Cyt C photoelectrochemical NO_2^- biosensors and sensing by other modes.

Electrode	[a]Analytical methods	Applied Potential (V)	Sensitivity ($\mu A\ \mu M^{-1}\ cm^{-2}$)	Linear range (μM)	Detection Limit (μM)	References
TiO_2(G) NW@EPNS/Cyt C	CA (PEC)	-0.11	201.79	0.5–9000	0.225	This work
MWCNTs-TiN/Cyt c/GC	CA	+0.92	121.5	1.0–2000	0.0014	(Haldorai et al., 2016)
SiO_2/Cyt c/SiO_2/BDD	CA	+0.70 (SCE)	0.17	–	0.5	(Geng et al., 2008)
Cyt c/DNA/MWNT/PAMAM/CS/GC	CA	+0.95 (SCE)	–	0.2–80	0.03	(Chen et al., 2010b)
Cyt c/L-cysteine/ P3MT/MWNT/GC	CA	+0.90	$7.04 \pm 0.07 \times 10^{-2}$	10–100	0.5	(Eguilaz et al., 2010)
PANI-g-ND/Au/cyt c	DPV	–	88.2	0.5–3000	0.16	(Gopalan et al., 2010)
Nafion/SLGnP–TPA–Mb film	CV	–	3.42×10^4	50–2500	10	(Yue et al., 2011)
Mb/Au-PTy-f-MWCNT/GCE	CA	+0.74	168	1.0–8000	0.002	(Vilian et al., 2015)
Nafion-BMIMPF6/Mb/ Carbon ionic liquid	CV	–	–	100–8400	50	(Sun et al., 2009)
Nafion/Hb/TiO_2NSs-rGO/GCE	CA	-0.7	–	1–2600	0.21	(Liu et al., 2015)
Hb-ZnO-Nafion/GCE	CA	- 0.675	–	10–2700	4.0	(Lu et al., 2008)
Hb-CS-DMF/GR/GCE	CA	-0.25 (SCE)	5.33	0.55 – 33	0.18	(Liu et al., 2011)
$BiVO_4$/FTO	CA (PEC)	+1.10	–	2.5–100	1.5	(Ribeiro et al., 2015)

[a] CA – chronoamperometry; PEC – photoelectrochemical; CV – cyclic voltammetry; DPV – differential pulse voltammetry.

3.6. Reproducibility, stability, and reusability

The reproducibility of the designed TiO_2(G) NW@EPNS/Cyt C biosensor was checked for the detection of 1 mM of NO_2^- using ten biosensors fabricated under the similar procedure and conditions. The TiO_2(G) NW@EPNS/Cyt C showed acceptable responses for the photocurrent with a relative standard deviation (RSD%) of 2.89%. Furthermore, the stability of TiO_2(G) NW@EPNS/Cyt C biosensor was also investigated. After using the electrode for sensing 1 mM of NO_2^- approximately 70 times over 30 days, the biosensor showed a marginal decrease ($<1\%$) in photocurrent. This ensures excellent stability for the TiO_2(G) NW@EPNS/Cyt C biosensor. To demonstrate the reusability of the proposed PEC biosensor for NO_2^- sensing using TiO_2(G) NW@EPNS/Cyt C, its electrochemical (DET for Cyt C) and PEC sensing characteristics were observed for 10 times in a day for the same fabricated biosensor over a period of 10 days. The biosensor was kept in double distilled water at 4 °C when not in use. After storing in distilled water, the DET of Cyt C was checked by cyclic voltammetry and the photocurrent was measured at −0.11 V under irradiation of light in the presence of 1 mM of NO_2^-. We observed two information. Foremost, the biosensor exhibited DET for Cyt C with nearly similar peak currents (~2% decrease after 100 repetitions) and redox characteristics that corresponded to DET of Cyt C. Secondly, the biosensors showed 97% of the photocurrent for 1 mM NO_2^- even after 100 repetitions as compared to the photocurrent observed for the first biosensing measurement. Therefore, we conclude that distilled water regenerates the biosensor activities without damage to its electrochemical and PEC properties. We envisage that the uses of biocompatible EPNS (containing water stable PMPA) and the photostable G included TiO_2 NW, contribute to the retrieval of biosensing properties. The fabricated biosensor is reusable for multiple (nearly 100) measurements.

3.7. Real sample analysis

As per the regulation for NO_2^- ions established by the United States Environmental Protection Agency (USEPA), the threshold value of NO_2^- in drinking water is 1.0 mg L^{-1}. Also, the world health organization (WHO) has set a maximum limit for NO_2^- at 3.0 mg L^{-1} for drinking water. Based on our results, the detection limit of NO_2^- at TiO_2(G) NW@EPNS/Cyt C PEC biosensor is much lower (LOD = 0.225 μM) than the limits set by USEPA and WHO for the determination of NO_2^-. To test the usefulness of the proposed TiO_2(G) NW@EPNS/Cyt C biosensor for NO_2^- detection in the practical samples, experiments were carried out with the practical samples (tap-water, milk and table salt). Recovery studies were done on practical samples by the addition of standard concentration of NO_2^-. The recovery percentage (%) of NO_2^- ranged from 99.57% to 100.1% (SI 10. Table), which suggested that TiO_2(G) NW@EPNS/Cyt C PEC biosensor is effective for the detection of NO_2^- in real samples. Redox reactions are possible in a few of the species such as metal ions and organic compounds, present in real samples (e.g: tap water) and that can have a profound influence on changing the concentration of the existing species either through redox transformation among themselves or through oxidation-redaction reactions between the species. The redox potentials, redox chemistry in aquatic system and kinetics of redox transformation, determine the concentration of the interconvertible redox sensitive species. In order to understand the influence of the few of the redox sensitive species on the NO_2^- biosensing performance of 1 mM of NO_2^- ions, we investigated the influence of $Fe^{(II)}/Fe^{(III)}$ (50 mM each), $Mn^{(II)}/Mn^{(IV)}$ (50 mM each) and organic systems such as aqueous NH_3 and dissolved O_2. The experimental results on PEC sensing of TiO_2(G) NW@EPNS/Cyt C revealed that the presence of the above mentioned redox species did not significantly change (~1% of initial) photocurrents.

4. Conclusions

In this work, a novel PEC biosensing platform is developed by modifying graphene (G) with an electroconductive polymer nanosponge (EPNS) and TiO_2 NW. The inclusions of G and TiO_2NW in EPNS along with immobilized Cyt C provide the basis for the construction of a highly sensitive and selective PEC biosensor for NO_2^-. Under the light irradiation, TiO_2(G) NW@EPNS/Cyt C PEC biosensor exhibits improved performances at a very low bias potential (−0.11 V). The TiO_2(G) NW@EPNS/Cyt C PEC NO_2^- biosensor has several unique advantages, such as lower bias voltage (−0.11 V), rapid response (~5 s), good sensitivity, excellent selectivity, wide linear range (0.5–9000 μM), good reproducibility, adequate stability and applicability for the detection of NO_2^- in real samples. The TiO_2(G) NW@EPNS/Cyt C biosensor exhibits improved performances which are primarily attributed to the synergistic roles of the components. We envisage that concept of the designing PEC biosensor platform with the composite material containing G, a photoactive material and a, polymer, is extendable towards the fabrication of biosensors for other analytes through judicious choices of the components and an enzyme.

Acknowledgements

This work was supported by the Priority Research Centers Program through a National Research Foundation of Korea (NRF) grant funded by the Ministry of Education, Science and Technology (2009–0093819) and a funded research project (NRF-2014R1A1A4A03004026).

Appendix A. Supplementary material

Supplementary data associated with this article can be found in the online version at http://dx.doi.org/10.1016/j.bios.2016.06.005.

References

Allen, M.J., Tung, V.C., Kaner, R.B., 2009. Chem. Rev. 110, 132–145.
Bartlett, R.L., Medow, M.R., Panitch, A., Seal, B., 2012. Biomacromolecules 13, 1204–1211.
Burda, C., Chen, X., Narayanan, R., El-Sayed, M.A., 2005. Chem. Rev. 105, 1025–1102.
Cao, W., Wei, C., Hu, J., Li, Q., 2008. Electroanalysis 20, 1925–1931.
Chen, D., Feng, H., Li, J., 2012. Chem. Rev. 112, 6027–6053.
Chen, D., Zhang, H., Li, X., Li, J., 2010a. Anal. Chem. 82, 2253–2261.
Chen, Q., Ai, S., Fan, H., Cai, J., Ma, Q., Zhu, X., Yin, H., 2010b. J. Solid State Electrochem. 14, 1681–1688.
Chen, Q., Ai, S., Zhu, X., Yin, H., Ma, Q., Qiu, Y., 2009. Biosens. Bioelectron. 24, 2991–2996.
Chen, X., Mao, S.S., 2007. Chem. Rev. 107, 2891–2959.
Chung, C., Kim, Y.K., Shin, D., Ryoo, S.R., Hong, B.H., Min, D.H., 2013. Acc. Chem. Res. 46, 2211–2224.
Dai, Z., Xu, X., Ju, H., 2004. Anal. Biochem. 332, 23–31.
Dickerson, R.E., Takano, T., Eisenberg, D., Kallai, O.B., Samson, L., Cooper, A., Margoliash, E., 1971. J. Biol. Chem. 246, 1511–1535.
Dinesh, B., Mani, V., Saraswathi, R., Chen, S.M., 2014. RSC Adv. 4, 28229–28237.
Ding, Y., Wang, Y., Li, B., Lei, Y., 2010. Biosens. Bioelectron. 25, 2009–2015.
Dobson, C.M., Šali, A., Karplus, M., 1998. Angew. Chem. Ed. 37, 868–893.
Doong, R.A., Shih, H.M., 2006. Biosens. Bioelectron. 22, 185–191.
Eguilaz, M., Agüí, L., Yanez-Sedeno, P., Pingarron, J.M., 2010. J. Electroanal. Chem. 644, 30–35.
Fujishima, A., 1972. Nature 238, 37–38.
Ge, J., Lei, J., Zare, R.N., 2011. Nano Lett. 11, 2551–2554.
Geim, A.K., Novoselov, K.S., 2007. Nat. Mater. 6, 183–191.
Geng, R., Zhao, G., Liu, M., Li, M., 2008. Biomaterials 29, 2794–2801.
Gnach, A., Lipinski, T., Bednarkiewicz, A., Rybka, J., Capobianco, J.A., 2015. Chem. Soc. Rev. 44, 1561–1584.
Gong, J., Wang, X., Li, X., Wang, K., 2012. Biosens. Bioelectron. 38, 43–49.
Gopalan, A.I., Lee, K.P., Komathi, S., 2010. Biosens. Bioelectron. 26, 1638–1643.
Guo, C.X., Li, C.M., 2010. Phys. Chem. Chem. Phys. 12, 12153–12159.
Haldorai, Y., Hwang, S.K., Gopalan, A.I., Huh, Y.S., Han, Y.K., Voit, W., Sai-Anand, G.,

Lee, Z., 2016. Biosens. Bioelectron. 79, 543–552.
Han, Z., Tang, Z., Li, P., Yang, G., Zheng, Q., Yang, J., 2013. Nanoscale 5, 5462–5467.
Kafi, A.K.M., Wu, G., Chen, A., 2008. Biosens. Bioelectron. 24, 566–571.
Kandimalla, V.B., Tripathi, V.S., Ju, H., 2006. Biomaterials 27, 1167–1174.
Khoshtariya, D.E., Wei, J., Liu, H., Yue, H., Waldeck, D.H., 2003. J. Am. Chem. Soc. 125, 7704–7714.
Koh, W.C.A., Rahman, M.A., Choe, E.S., Lee, D.K., Shim, Y.B., 2008. Biosens. Bioelectron. 23, 1374–1381.
Komathi, S., Sai-Anand, G., Gopalan, A.I., Lee, H.G., Yeo, H.K., Kang, S.W., Lee, K.P., 2016. Sens. Actuators B: Chem. 228, 737–747.
Lee, H.G., Sai-Anand, G., Komathi, S., Gopalan, A.I., Kang, S.W., Lee, K.P., 2015a. J. Hazard. Mater. 283, 400–409.
Lee, H.G., Gopalan, A.I., Sai-Anand, G., Lee, B.C., Kang, S.W., Lee, K.P., 2015b. Mater. Chem. Phys. 154, 125–136.
Lee, K.P., Gopalan, A.I., Komathi, S., 2009. Sens. Actuators B Chem. 141, 518–525.
Léger, C., Bertrand, P., 2008. Chem. Rev. 108, 2379–2438.
Li, H., Li, J., Xu, Q., Yang, Z., Hu, X., 2013. Anal. Chim. Acta 766, 47–52.
Li, H., Li, M., Guo, W., Di, H., Fang, C., Yang, B., 2014a. J. Solid State Electrochem. 18, 477–485.
Li, X.N., Yuan, Z., He, S.G., 2014b. J. Am. Chem. Soc. 136, 3617–3623.
Li, X., Chen, Y., Kumar, A., Mahmoud, A., Nychka, J.A., Chung, H.J., 2015. ACS Appl. Mater. Interfaces 7, 20753–20760.
Lin, M., Lu, D., Zhu, J., Yang, C., Zhang, Y., Liu, Z., 2012. Chem. Commun. 48, 3315–3317.
Liu, H., Duan, C., Yang, C., Shen, W., Wang, F., Zhu, Z., 2015. Sens. Actuator B-Chem. 218, 60–66.
Liu, H., Hill, H.A.O., Chapman, S.K., 2001. J. Electroanal. Chem. 500, 598–603.
Liu, P., Zhang, X.H., Feng, L.J., Xiong, H.Y., Wang, S.F., 2011. Am. J. Biomed. Sci. 3, 69–76.
Loh, K.P., Bao, Q., Eda, G., Chhowalla, M., 2010. Nat. Chem. 2, 1015–1024.
Lu, X., Zhang, H., Ni, Y., Zhang, Q., Chen, J., 2008. Biosens. Bioelectron. 24, 93–98.
Margoliash, E., Frohwirt, N., Wiener, E., 1959. Biochem. J. 71, 559.
Moretto, L.M., Bertoncello, P., Vezza, F., Ugo, P., 2005. Bioelectrochemistry 66, 29–34.
Mou, Z., Wu, Y., Sun, J., Yang, P., Du, Y., Lu, C., 2014. ACS Appl. Mater. Interfaces 6, 13798–13806.
Nalampang, K., Panjakha, R., Molloy, R., Tighe, B.J., 2013. J. Biomater. Sci. Polym. Ed. 24, 1291–1304.
Noll, T., Noll, G., 2011. Chem. Soc. Rev. 40, 3564–3576.
Novoselov, K.S., Geim, A.K., Morozov, S.V., Jiang, D., Zhang, Y., Dubonos, S.A., Grigorieva, I.V., Firsov, A.A., 2004. Science 306, 666–669.
Ohno, N., Cusanovich, M.A., 1981. Biophys. J. 36, 589.
Peng, H.P., Liang, R.P., Qiu, J.D., 2011. Biosens. Bioelectron. 26, 3005–3011.
Qiao, Y., Bao, S.J., Li, C.M., Cui, X.Q., Lu, Z.S., Guo, J., 2007. Acs Nano 2, 113–119.
Qiu, B., Xing, M., Zhang, J., 2014. J. Am. Chem. Soc. 136, 5852–5855.
Ribeiro, F.W.P., Moraes, F.C., Pereira, E.C., Marken, F., Mascaro, L.H., 2015. Electrochem. Commun. 61, 1–4.
Ronkainen, N.J., Halsall, H.B., Heineman, W.R., 2010. Chem. Soc. Rev. 39, 1747–1763.
Sasaki, T., Watanabe, M., 1997. J. Phys. Chem. B 101, 10159–10161.
Shie, J.W., Yogeswaran, U., Chen, S.M., 2008. Talanta 74, 1659–1669.
Sun, W., Li, X., Wang, Y., Li, X., Zhao, C., Jiao, K., 2009. Bioelectrochemistry 75, 170–175.
Tokudome, H., Yamada, Y., Sonezaki, S., Ishikawa, H., Bekki, M., Kanehira, K., Miyauchi, M., 2005. Appl. Phys. Lett. 87, 213901–214100.
Vilian, A.E., Veeramani, V., Chen, S.M., Madhu, R., Kwak, C.H., Huh, Y.S., Han, Y.K., 2015. Sci. Rep. 5, 18390.
Wang, J., Li, M., Shi, Z., Li, N., Gu, Z., 2002. Anal. Chem. 74, 1993–1997.
Wang, J., Musameh, M., Lin, Y., 2003. J. Am. Chem. Soc. 125, 2408–2409.
Wang, P., Dai, W., Ge, L., Yan, M., Ge, S., Yu, J., 2013. Analyst 138, 939–945.
Williams, G., Seger, B., Kamat, P.V., 2008. ACS Nano 2, 1487–1491.
Wilson, N.R., Pandey, P.A., Beanland, R., Young, R.J., Kinloch, I.A., Gong, L., Liu, Z., Suenaga, K., Rourke, J.P., York, S.J., Sloan, J., 2009. ACS Nano 3, 2547–2556.
Xiang, Q., Yu, J., Jaroniec, M., 2012. J. Am. Chem. Soc. 134, 6575–6578.
Xu, Q., Mao, C., Liu, N.N., Zhu, J.J., Sheng, J., 2006. Biosens. Bioelectron. 22, 768–773.
Xu, X., Pan, L., Liu, Y., Lu, T., Sun, Z., Chua, D.H., 2015. Sci. Rep. 5, 8458.
Yamamoto, H., Liu, H., Waldeck, D.H., 2001. Chem. Commun. 11, 1032–1033.
Yan, Y., Zheng, W., Su, L., Mao, L., 2006. Adv. Mater. 18, 2639–2643.
Younathan, J.N., Wood, K.S., Meyer, T.J., 1992. Inorg. Chem. 31, 3280–3285.
Yue, R., Lu, Q., Zhou, Y., 2011. Biosens. Bioelectron. 26, 4436–4441.
Zhang, Y., Chen, X., Yang, W., 2008. Sens. Actuators B: Chem. 130, 682–688.
Zheng, Z., Zhou, Y., Li, X., Liu, S., Tang, Z., 2011. Biosens. Bioelectron. 26, 3081–3085.
Zhu, A., Tian, Y., Liu, H., Luo, Y., 2009. Biomaterials 30, 3183–3188.
Zhu, Z., Qu, L., Niu, Q., Zeng, Y., Sun, W., Huang, X., 2011. Biosens. Bioelectron. 26, 2119–2124.

Please cite this article as: Muthuchamy, N., et al., Biosensors and Bioelectronics (2016), http://dx.doi.org/10.1016/j.bios.2016.06.005